

Richard F. Spaide

The choroid is situated between the sclera and Bruch's membrane and most of its substance is occupied by blood vessels; more than 70 % of all of the blood flow to the eye goes to the choroid [1]. The photoreceptors have the highest rate of oxygen use per unit weight of tissue in the body [2], and nearly all of that is accounted for by the mitochondria of the inner segments. The retinal circulation, which is about 5 % of the blood flow to the eye, supplies the inner retina, but the choroid supplies the oxygen used by the outer retina, including the inner segments. The choroid is the only source for the avascular fovea. The choroid has additional functions including acting as a heat sink [3], absorbing stray light, participating in immune response and host defense [4], and is an integral part in the process of emmetropization [5]. Although the ocular manifestations of high myopia have become apparent over the past centuries, appreciation of the abnormalities within the choroid has occurred only recently. High myopia is associated with profound changes in the choroid that are important in the pathogenesis of many important visually significant abnormalities. Advances in imaging have greatly increased our ability to visualize the choroid, providing an opportunity to better understand the choroid in health and disease.

9.1 The Embryology and Anatomy of the Choroid

9.1.1 Embryology

Each optic vesicle forms as outpouching of the forebrain. This vesicle invaginates to form a double-walled optic cup. The inner layer of the cup is destined to form the retina and

R.F. Spaide, MD
Vitreous, Retina, Macula Consultants of New York,
460 Park Ave, 5th Floor,
New York, NY 10021, USA
e-mail: rickspaide@gmail.com

the outer layer, the retinal pigment epithelium (RPE). The inferior portion of the cup initially has a gap that forms the choroidal fissure, which allows access for the hyaloid artery to enter the eye. Eventually the gap closes. The uvea develops from the mesoderm and migrating neuroectoderm that surround the optic cup. Mesodermal cells start to differentiate into vessels around the same time that the RPE appears. The choriocapillaris starts to form at about the fifth to sixth week. The basal lamina of the RPE and of the choriocapillaris defines the boundaries of the developing Bruch's membrane by week 6 [6]. The choriocapillaris becomes organized with luminal networks well before the rest of the choroidal vasculature develops. The posterior ciliary arteries enter the choroid during the eighth week of gestation, but it takes until week 22 before arteries and the veins become mature. Melanocyte precursors migrate into the uveal primordia from the neural crest at the end of the first month but start differentiating at the seventh month. The pigmentation of the choroid begins at the optic nerve and extends anteriorly to the ora serrata. This process is complete by about 9 months [7]. The sclera is derived from mesenchymal condensation starting anteriorly and completing posteriorly by week 12.

9.1.2 Choroidal Anatomy

The choroid is an unusual structure primarily composed of blood vessels but also has connective tissue, melanocytes, and intrinsic choroidal neurons. Birds have fluid-filled lacunae identified as true functional lymphatic system in their choroid [8]. Although humans don't have a lymphatic system in the eye, Schroedl and associates found human choroids have macrophage-like cells that stain positively for a lymphatic endothelium-specific marker, lymphatic vessel endothelial hyaluronic acid receptor [9]. Humans also have cells with nonvascular smooth muscle-like elements in the choroid [10, 11]. These cells are located around the entry of posterior ciliary vessels and nerves, along the vessels in the posterior segment, and under the foveal region. It has been

proposed the arrangement suggests the cells, which have actin contractile elements, may help stabilize the position of the fovea during accommodation [12]. The human choroid has intrinsic choroidal neurons, which have been theorized to participate in autoregulation of blood flow [13]. The choroid is attached to the sclera by strands of connective tissue which are easily separated anteriorly creating a potential space between them, the suprachoroidal space.

The blood from the short PCAs enters the eye and travels through successively smaller branches of arterioles within the choroid. The choroid is traditionally thought to be arranged in layers of vessels from the outer to inner part of the choroid labeled as Haller's layer, Sattler's layer, and the choriocapillaris. Haller's layer contains larger choroidal vessels, while Sattler's layer has medium-sized vessels that branch inwards to supply the choriocapillaris. There is no distinct border between Haller's and Sattler's layers or even an established definition of what is meant by large or medium. In actuality Sattler thought there were remnants of a tapetum in humans. He proposed this was in the middle choroid, and initially the term Sattler's layer wasn't used to designate the blood vessels. The blood then enters the choriocapillaris, a densely packed monolayer of fused large-bore fenestrated capillaries. The network of vessels in the choriocapillaris is tightly packed in the posterior portion of the eye, but the structure becomes looser in the periphery. The vitality of the choriocapillaris is maintained in part by constitutive secretion of vascular endothelial growth factor (VEGF) by the RPE [14]. The choriocapillaris is highly polarized [15] with the internal surface having multiple localized areas of thinning of the capillary wall known as fenestrations. These thinner areas appear to facilitate the passage of material out of the capillaries and direct the flow toward the RPE. The number of fenestrations is more prominent in the submacular area as compared with the mid- or far periphery [16]. Similarly sized vessels in the retina do not have fenestrations. Soluble VEGF isoforms are required for fenestrations to occur in the choriocapillaris [14], and these fenestrations disappear with VEGF withdrawal [17]. In experimental myopia the choriocapillaris becomes less dense (Fig. 9.1), with decreased capillary lumens and a loss of fenestrations [18]. Also in myopes, as will be seen, the choroid is thinner than in emmetropes and the vascular diameter of larger choroidal blood vessels is less as well.

Blood from the choriocapillaris collects into venules that lead into larger venules that course in the outer choroid toward the ampulla of the vortex veins. The typical vortex vein passes obliquely through the sclera for a distance of about 4.5 mm as it exits the eye. Some drainage of the anterior choroid occurs through the anterior ciliary veins into the ciliary body. There are often four vortex veins per eye, with the ampulla of the vortex veins lying at the equator of the

eye. The number can range from three to eight [19]; in high myopes there is often more than four and there may be posterior vortex veins known as ciliovagal veins, which drain near or through the optic nerve foramen (Fig. 9.2) [20]. The number and configuration of vortex veins is different in myopia; since myopia develops over time, the implication is that what appears to be additional vortex veins in myopia is acquired. The vortex veins drain into the superior and inferior ophthalmic veins [21].

9.2 Blood Flow Within the Choroid

Hayreh discovered many of the fascinating features of the choroidal blood flow from his observations of humans and monkeys [22]. The choroidal arteries do not anastomose with one another and each behaves like an end artery. There are no direct anastomoses between the PCAs or in arterial supply within the choroid. There is potential for local flow alterations to occur in the choriocapillaris based on pressure fluctuations. Once the blood leaves the choriocapillaris, it enters another segmented system the venous outflow from the eye. The segmentation of the venous system is different from that of the arterial system.

In the early phase of fluorescein angiography, it is common to see areas of the choroid that do not appear to fill with dye as quickly as adjacent regions. The pressure of the blood is reduced from about 75 % of the systemic blood pressure at the short PCAs to that in the choriocapillaris, which has been measured in rabbits to be approximately 5–9.5 mmHg greater than the intraocular pressure [23]. The efferent and afferent vessels set up pressure gradients within the choriocapillaris to create a lobular flow. The flow characteristics are thought to be more dependent on complex gradients rather than anatomic patterns strictly dictated by choriocapillaris anatomy [24]. The designation of a watershed filling defect is made if the region of choroidal filling is delayed past the laminar flow stage of the retinal veins [25]. A common appearance of a watershed zone is a stripe, one to several millimeters wide, running vertically at the temporal border of the optic disc in which the choroid is not as hyperfluorescent as surrounding areas [22]. This watershed zone is thought to be the boundary between areas of the choroid supplied by the medial and lateral PCAs. Eyes with more than two PCAs have more watershed zones, with a vertical stripe involving the optic nerve region and a number of radiating lines extending from the nerve seen dependent on the actual number of PCAs. Venous watershed zones exist for the venous circulation and form a cruciate pattern centered slightly temporal to the optic nerve [22]. In times of decreased perfusion, watershed zones may represent the regions with the poorest flow since they are at the shared boundaries of non-overlapping systems. The peripapillary choroid is a very important region of the

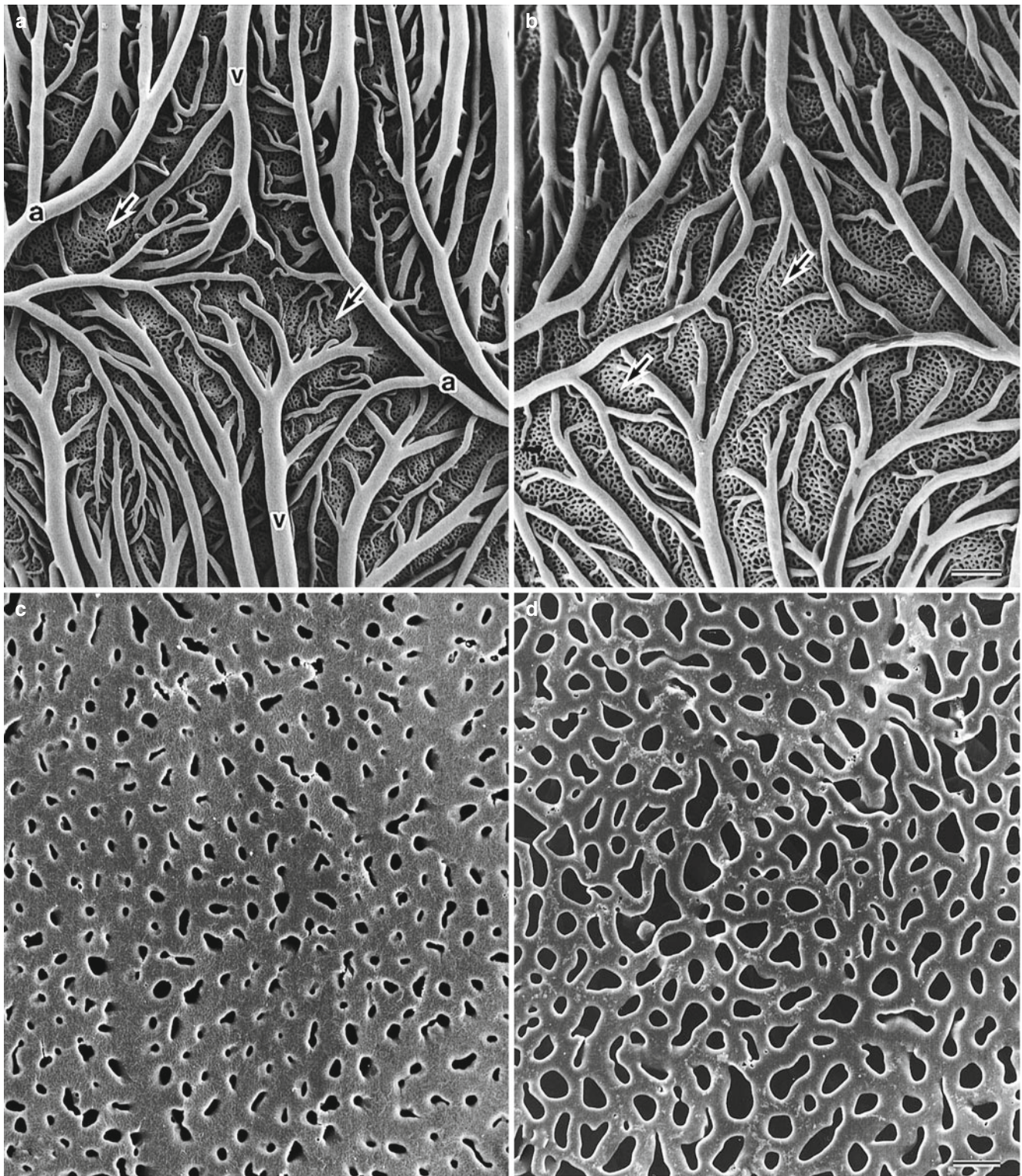


Fig. 9.1 Scanning electron micrographs of corrosion casts of the choroidal vasculature in control and myopic chick eyes at the fourth week. **(a, b)** The control eye (left) has a greater vascular density of larger vessels serving the choriocapillaris (*arrows*) than the myopic eye. The arterioles are designated by (*a*) and the venules (*v*). **(c)** The

choriocapillaris seen en face in a control eye has the expected high vascular density. **(d)** In a representative myopic eye, the individual vessels of the choriocapillaris have a lower packing density, and the vessels are smaller and more tubelike (Derived from Hirata and Negi [18])

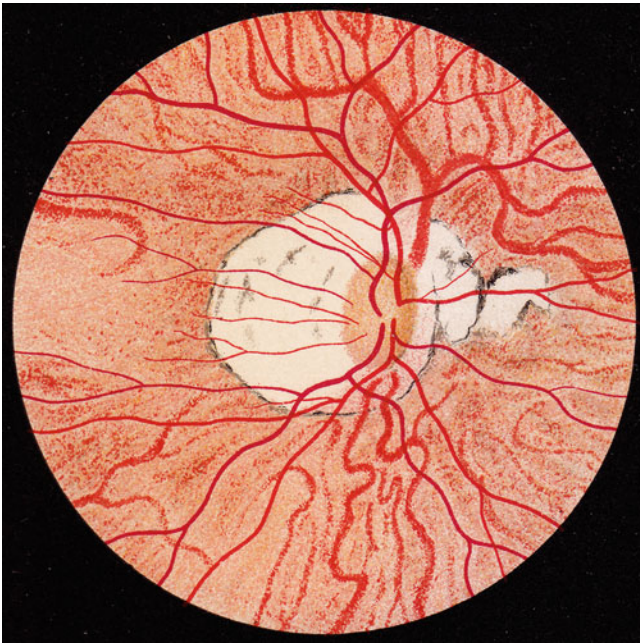


Fig. 9.2 Otto Haab, a prominent Swiss ophthalmologist, described posterior venous drainage in high myopes and called the vessels posterior vortex veins, a name still used today. In this color drawing, taken from the third edition of Haab's atlas, a prominent vein is seen to exit the choroid superonasal to the nerve. Two smaller vessels are seen at the inferior border of the nerve. The drawing is an accurate reflection of the posterior venous drainage in high myopes. Unlike the typical vortex veins in the periphery, the posterior vortex veins do not have an ampulla or a spray of contributing vessels

choroidal vascular bed because of its important role in the blood supply of the anterior part of the optic nerve, including the optic disc [26].

9.3 The Regulation of Choroidal Blood Flow

Although almost every tissue in the body has some form of autoregulation, the extent of the autoregulation of the choroid is controversial and contradictory. Some investigators have shown the choroid has no autoregulation when the perfusion pressure gradient is decreased by raising the intraocular pressure (IOP) [27, 28]. Other investigators have shown the choroidal blood flow varies with IOP, perfusion pressure [29], endogenous nitric oxide production [30], and vasoactive secretory production of choroidal ganglion cells [31]. Various studies have suggested the choroid has some autoregulatory capacity during changes in ocular perfusion pressure [32–34]. Moreover, Polska and associates found that the mechanisms regulating choroidal blood flow in the human fovea compensate better for an increase in arterial blood pressure than for an increase in intraocular pressure [32].

Autoregulation in regular tissues usually keeps the oxygen partial pressure at a relatively low level but the inner choroid's oxygen partial pressure is so high that it is likely that the choroidal circulation is regulated by other factors. For example, CD-36 is a scavenger receptor expressed in the basal RPE. Houssier and associates showed that CD-36-deficient mice fail to induce COX-2 and subsequent VEGF synthesis at the level of the RPE and develop progressive degeneration of the choriocapillaris [35]. Therefore, CD-36 binding by the RPE, such as what happens in the normal process of phagocytosis of the photoreceptor outer segments, seems to be one of the factors maintaining the vessels of the inner choroid.

One explanation for what may appear to be incomplete autoregulation is that the choroidal blood flow is much higher than in other tissues and has a low oxygen extraction ratio. Autoregulation is an adaptive compensatory mechanism to adjust blood flow according to the local needs of the tissue supplied. The high oxygen partial pressure and low oxygen extraction imply, though, that the flow in the choroid is maintained at a level much greater than the local needs of the choroid or RPE would ordinarily seem to dictate. On the other hand, the O_2 delivered to the outer retina is consumed in its entirety by the mitochondria in the inner segments of the photoreceptors. It seems unlikely that a direct feedback mechanism exists between the oxygen utilization by the inner segments of the photoreceptors and the choriocapillaris as diseases that cause acute destruction of the outer retina such as acute zonal occult outer retinopathy are not associated with decreased thickness of the choroid [36]. There are likely to be indirect trophic mechanisms that haven't been elucidated so far.

9.4 Other Choroidal Functions

There have been other reasons proposed for the large blood flow in the choroid. The amount of light energy delivered to the retina by incoming light is insufficient to cause a significant elevation in temperature and thus is an unlikely explanation [37]. It is possible that the high metabolism in the outer retina may produce enough heat to require mechanisms to reduce the local temperature. The high blood flow may help conduct heat away from the outer retina/RPE complex. The choroid contains melanocytes which improve optical function by absorbing scattered light and may also indirectly protect against oxidative stress. These melanocytes exist in an environment of high O_2 partial pressure, which along with the light exposure may be a risk factor for malignant transformation to melanoma. Melanocytes in human RPE are particularly rich in zinc and may serve as a reservoir for this metal ion [38–40].

9.5 Imaging the Choroid

Because of its localization between the overlying pigmented RPE and the underlying opaque and rigid fibrous sclera, the choroid is difficult to visualize with conventional imaging. Methods employing light reflection or fluorescence generation are impeded by the pigment in the RPE and choroid. Conventional OCT is affected by the effects of melanin and also the scattering properties of the blood and blood vessels. The choroid is a deeper structure and the depth affects the detection sensitivity.

9.5.1 Angiography

Fluorescein is stimulated by blue light with a wavelength between 465 and 490 nm and emits at a green light with the peak of the emission spectral curve ranging between 520 and 530 nm and a curve extending to approximately 600 nm. Both the excitation and emission spectra from fluorescein are blocked in part by melanin pigment, which acts to decrease visualization of the choroid. Fluorescein extravasates rapidly from the choriocapillaris and fluoresces in the extravascular space, and this also prevents delineation of the choroidal anatomy. The analysis of the choroid using fluorescein angiography is also limited by light absorption and scattering by the pigment in the RPE and choroid and by the blood in the choroid. Gross filling of the choroid can be seen, as can the converse, choroidal filling defects. Diseases causing arteritis such as giant cell arteritis or Wegener's granulomatosis can cause regions of decreased perfusion of the choroid. The actual visualization of the various vessels in the choroid is not practical with fluorescein angiography. Therefore estimations of vascular density of the choroid are not easily done. On the other hand, fluorescein angiography is ideal for visualizing retinal vascular abnormalities and many forms of choroidal neovascularization (CNV), particularly classic CNV.

Indocyanine green (ICG) absorption peak is between 790 and 805 nm and it fluoresces in a somewhat longer wavelength range, depending on the protein content and pH of the local environment. The longer wavelengths used have the attribute of penetrating the pigmentation of the eye better than the wavelengths used with fluorescein angiography. The retinal pigment epithelium and the choroid absorbs up to 75 % of blue-green light used for fluorescein angiography but only up to 38 % of the near-infrared light used for ICG angiography [41]. ICG is 98 % protein bound, with 80 % binding to larger proteins such as globulins and alpha-1-lipoproteins [42, 43]. The amount of fluorescence derived from ICG during typical angiographic examination is much less than that obtained from fluorescein, and the resultant light is in the near-infrared wavelengths. Because of the poor

sensitivity to near-infrared light by photographic film, the first practical imaging of ICG fluorescence in the clinic awaited commercial availability of digital charge-coupled devices (CCDs).

ICG is highly protein bound, so there is less opportunity for the dye to leak from the normal choroidal vessels. During the earlier phases of ICG angiography, the choroidal vessels are visible. The vertical summation of the choroid is seen, making it difficult to delineate individual layers of vessels. Over the course of the angiogram, some staining of the extravascular tissue particularly Bruch's membrane occurs, obscuring visualization of deeper structures. This means flow can be estimated by looking at the early frames of the ICG angiogram, but later phases can't be used for the same purpose.

Early after the availability of ICG angiography, many diseases were investigated, and new information that was not obtainable by fluorescein angiography was generated. Much of this information was interesting from a research standpoint, but did not have practical clinical utility. For real-world use ICG is most helpful in diagnosing and evaluating polypoidal choroidal vasculopathy and central serous chorioretinopathy. Secondary uses include evaluation of choroidal inflammatory diseases, angioid streaks, choroidal tumors, and in providing rough estimates of choroidal blood flow. The advent of widespread use of autofluorescence imaging and optical coherence tomography (OCT) methods to evaluate the choroid has largely supplanted ICG angiography for these secondary uses.

9.5.2 Ultrasonography

Contact b-scan ultrasonography typically uses a 10 MHz probe placed on the eyelid. The probe used contains a piezoelectric crystal that is stimulated to vibrate by a short duration of an electrical driving current. Reflected sound waves cause the crystal to vibrate, which through the piezoelectric effect causes an electrical current. Sound decreases in intensity with increasing distance because of divergence of the sound beam and attenuation of the sound by the intervening tissue. Thus reflected sound waves vary in strength with the depth of the reflecting structure in the eye. To compensate for the decrease in signal strength with time of flight, the gain of the amplifier is increased over the detection interval. Depth information is derived directly from time-of-flight information and the speed of sound through the medium involved. The direction of the crystal then is rotated slightly by a motor within the probe to successively build a two-dimensional image, a b-scan.

Although each a-scan is shown as a needle thin line within the b-scan image, the actual situation is far different. The

piezoelectric crystal has some focusing ability, but in reality the sound beam produced by a piezoelectric crystal in a conventional b-scan probe has a main lobe and several side lobes [44]. Even the main lobe can be 1 mm in diameter at the surface of the retina. The side lobes add to the ambiguity of the reflection as does scattering within the eye. Given the eye is a curved structure, the wide probing beam produces a returning echo from any given region in the posterior portion of the eye that is smeared over an interval of time. The wavelengths used in ultrasonography dictate a theoretical axial resolution of about 150 μm , but the actual resolution in clinical use the resolution is much lower. For example, a typical b-scan of the optic nerve will not show the cup unless there is a very high cup to disc ratio because of the broad diameter of the sample imaged. Another significant problem with ultrasonography is the exact location of the image obtained is not known. The general region can be estimated by evaluating relationships with neighboring structures and by trying to imagine where the probe is aimed.

In non-pathologic conditions the reflectivity of the choroid is difficult to distinguish from the overlying retina and the underlying sclera. In high myopes the thickness of the choroid can easily be less than the resolution of contact b-scan ultrasonography, making any meaningful imaging of the choroid in populations of high myopes impossible. Contact b-scan ultrasonography is useful to examine the general contour of the eyewall and to visualize staphylomata.

9.6 Optical Coherence Tomography

9.6.1 Interferometry

In dry air, the speed of sound is 343.2 m/s. The sound velocity in an average phakic eye is 1,555 m/s [45]. This means that the time it takes sound to travel the length of a phakic eye with an axial length of 24 mm is approximately 15.4 μs , which is easy to measure. Because light travels very rapidly (3×10^8 m/s), it is not possible to measure the time-of-flight delay on a micron-scale level of resolution using an external system of time measurement. The time it takes light to travel a micron is the same or less than it would take an electron to travel the same distance in an electronic circuit. Measurement of multiple reflections with a detector and the subsequent required electronic circuitry requires conduction paths for electrons that are much longer than the variations in path length of the light rays. However, light rays have a repeating characteristic inherent in their own wave properties. A clever way to time how long light takes to travel a given distance is to use the wave-like character of the light itself as its own internal clock. Phase differences in waveforms can be detected and reveal very small changes in time of flight. That is what a Michelson interferometer does; the wavelength of

the light is used as its own timing standard. The micron-scale resolution is achieved by comparing the time of flight of the sample reflection with the known delay of a reference reflection by using interference to find phase differences in the light waves.

Coherency of light is a measure of how correlated one wave of light is with another. Temporal coherency is a measure of how correlated one wave of light is with another generated at a different time. Coherence length is the distance light would travel during the coherence time. Light produced by a conventional laser has a long coherence time because one wave of light is similar to other waves of light produced at times before or after. It is possible to produce light with a short coherence length. In this situation the waveform of light produced is the same for all of the light rays produced at any one instance, but this waveform is different from other waveforms produced at other times. This approach essentially puts a time stamp on the waveform. Low-coherence light split into a reference arm can only interfere with light from the sample arm if the path lengths are the same or are nearly the same.

In time-domain OCT each point in the tissue is sampled one at a time. The probing beam illuminates the tissue, but information is obtained from a small portion of the tissue at any given instant. This means time-domain OCT is less efficient at extracting information from tissue at any given total light exposure. The total amount of light that can be delivered to tissue is limited by safety standards. Spectral-domain (SD) OCT takes the light from the interferometer and passes it through a grating to separate out the component wavelengths. Using a Fourier transform it is possible to determine where, and how strongly, different reflections in the sample arm originated from simultaneously. In effect all layers produce signal during each a-scan. Because of this feature SD-OCT devices are much more efficient at extracting information from tissue at any given light exposure. This increase in efficiency is often translated to increased scanning speeds such that SD-OCT instruments typically scan the eye with speeds up to 100 times faster than time-domain OCT instruments. There are some problems inherent in SD technology. The deeper tissues produce higher frequency signals, but the way the grating and detector sample this frequency is not linear. The higher frequencies are bunched together to a greater extent than lower frequencies. In addition the sensitivity of the detection decreases with increasing frequency. This causes SD-OCT to have decreasing sensitivity and resolution with increasing depth.

A consequence of the decreasing sensitivity is the choroid cannot be imaged in many emmetropes with conventional SD-OCT. Eyes with high myopia have thinner choroids and a relative depigmentation, making it possible to visualize the full thickness of the choroid in many eyes with conventional SD-OCT. Because a Fourier transform is used,

two conjugate images are developed from the interferometric signal. In practical use only one of these two images are shown, typically with the retina facing toward the top of the screen. If the peak sensitivity is placed posteriorly typically at the inner sclera, deeper structures such as the choroid can be seen. The upside down conjugate image of these structures is visualized and the right side-up image of structures in the orbit is blank because of the lack of any reflected imaging information. This method of imaging the choroid is called enhanced depth imaging (EDI) OCT [46]. It is now simply performed with SD-OCT instruments, often by just selecting EDI in the software of the instrument. To improve the signal-to-noise ratio and therefore image appearance, many b-scans can be averaged together, typically using 50–100 images. Segmentation of OCT images allows visualization and measurement of various layers in the eye. In high myopes the choroid can be extremely thin, making it difficult to segment volume scans without attendant segmentation errors.

Swept-source OCT (SS-OCT) uses a frequency-swept light source and detectors, which measure the interference output as a function of time [47, 48]. The sensitivity of SS-OCT varies with depth as well, but the roll-off in sensitivity is not as great as seen with SD-OCT. In addition SS-OCT uses a longer center wavelength, which has improved ability to penetrate through tissue. Therefore both the vitreous and choroid can be imaged simultaneously; there is no need to pick one or the other. There are trade-offs with swept-source OCT that have to be considered. Although longer wavelengths of light may penetrate tissue to a greater degree, the problem is water absorbs longer wavelengths of light. This restricts the range or bandwidth of wavelengths that can be used in the eye, since the vitreous is mostly water. Increasing the center wavelength has the effect of decreasing the resolution for any given bandwidth. Water absorption of longer wavelengths is an important impediment to expanding the bandwidth of current 1 μm swept light sources, which limits the ability to overcome the decrease in resolution by increasing the bandwidth. Newer light sources operating at shorter wavelengths are being developed, and these light sources may avoid the problem of water absorption. For example, a SS-OCT using a large bandwidth light source with a center wavelength of 850 nm could provide very high speed, high resolution imaging with potentially less falloff in sensitivity with depth as compared with SD-OCT implementations.

No matter what the imaging modality is, high myopia represents special challenges for OCT. The extreme axial length of highly myopic eyes can represent difficulties in obtaining a usable image. The posterior portion of the highly myopic eye often has staphylomata and curvatures of the eyewall appear exaggerated in OCT renderings. The zone in which images are obtained in most commercial OCT instruments is

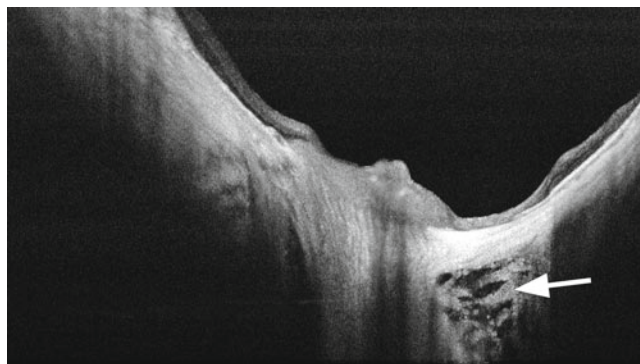


Fig. 9.3 Swept-source OCT is able to provide visualization of the subarachnoid space if there is peripapillary atrophy, which there usually is, particularly in the region of the conus [99]. Note the beams of tissue visible (arrow)

approximately 2 mm. Wide-angle scans image enough of the extent of a highly myopic eye that the vertical range of tissue can exceed the 2 mm window. Imaging of the areas outside of this 2 mm are seen as upside down conjugates. This produces artifactual image folding or mirroring. Imaging high myopes presents interesting opportunities however. The choroid is thin and does not have much pigment, so with EDI-OCT or SS-OCT it is possible to visualize the full thickness of the sclera and even to see into the subarachnoid space around the optic nerve (Fig. 9.3).

9.7 Measurements and Reproducibility of Choroidal Thickness

There is a very good intersystem [49, 50], interobserver, and intervisit reproducibility [50] of manual choroidal thickness measurements. The interobserver repeatability is good using EDI-OCT [16, 46, 50, 51], Cirrus HD-OCT [49, 52], Optovue RTVue [16], and SS-OCT [50, 53]. The intersystem reproducibility of choroidal thickness measurements has been assessed between EDI-OCT and SS-OCT [50] and also between three different SD-OCT devices: Cirrus HD-OCT, Spectralis using EDI module, and RTVue [49]. Tan and associates found the intraclass correlation coefficient for interobserver reproducibility of 0.994 but also the value of the mean difference between choroidal thickness measurements between graders that was 2.0 μm for 24 normal eyes of 12 healthy subjects [51]. These levels of agreement are smaller than the diurnal variation in choroidal thickness in humans [51]. Automated segmentation methods are generally faster but substitute idiosyncrasies and biases of the coded algorithm for idiosyncrasies and biases of a human observer. Wide area thickness maps and volume calculations are in beta testing stages at present and should be available in the near future.

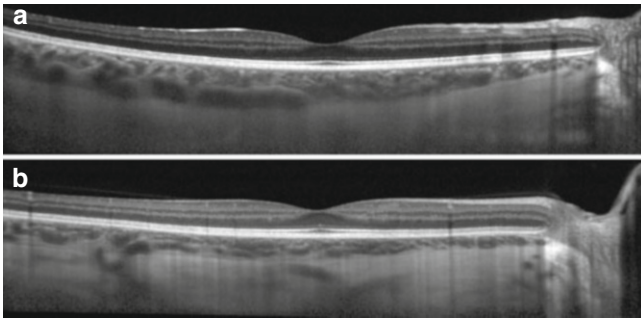


Fig. 9.4 Choroidal thickness in (a) a 31-year-old emmetrope and (b) a 29-year-old -6 myope. Note the subfoveal choroidal thickness is decreased in the myope as compared with the emmetrope despite their relatively young ages

9.8 Normal Subfoveal Choroidal Thickness

Margolis and Spaide investigated 54 normal, non-myopic eyes with a mean age of 50.4 years using the EDI-OCT and reported a mean subfoveal choroidal thickness of $287\ \mu\text{m}$ (Fig. 9.4a) [54]. Normal was defined as patients without any significant retinal or choroidal pathologic features, uncontrolled diabetes or hypertension, and a refractive error less than 6 diopters of spherical equivalent. The choroidal-scleral interface has been identified in 100 % of subjects in this study [54]. The authors showed that increasing age was correlated significantly with decreasing choroidal thickness at all points measured. The subfoveal choroidal thickness was found to decrease by $15.6\ \mu\text{m}$ for each decade of age [54]. Ikuno and associates investigated 86 non-myopic eyes of healthy Japanese patients with SS-OCT with a mean age of 39.4 years and found a subfoveal choroidal thickness of $354\ \mu\text{m}$. Ikuno and associates found that the choroidal thickness decreased by $14\ \mu\text{m}$ for each decade of age [55]. The mean subfoveal choroidal thickness has been found to vary among studies from $203.6\ \mu\text{m}$ in 31 eyes with a mean age of 64.6 years [53] to $448.5\ \mu\text{m}$ in 22 eyes with a mean age of 35.7 years [56]. The refractive error and age has to be taken into account, as does diurnal variation, making comparison of general mean values impossible for many studies. These comparisons are further hindered by some studies reporting choroidal thickness in patient groups using techniques that could not visualize the choroidal-scleral junction in all eyes. The percentage of identification of the choroidal-scleral interface was 74 % of 34 eyes in one series using SD-OCT [52], for example. Some studies excluded patients with ocular disorders [52–54], some excluded patients with ocular and systemic disorders [55, 57], and some mentioned they excluded patients with systemic disorders that might affect choroidal thickness [53, 54]. Even though these studies

propose to evaluate normal eyes, some of them included highly myopic eyes with a spherical equivalent error greater than -6 diopters [53, 57, 58].

There are several possible reasons for the decrease in subfoveal choroidal thickness with age, such as loss of choriocapillaris, a decrease in the diameter of the choriocapillary vessels, decrease in luminal diameter of blood vessels, and, in some cases, a diminution of the middle layer of the choroid [52, 59, 60]. Histologic evaluation of eye bank and autopsy eyes found a yearly decrease in choroidal thickness of $1.1\ \mu\text{m}/\text{year}$, which was less than the amount measured in vivo [54]. The differences may be related to measurement technique as the histologic specimens were measured in autopsy eyes, which by default had no blood pressure and the choroid is an inflated structure [59–61].

The choroidal thickness has also been found to fluctuate with defocus in humans [62]. Maintenance of emmetropia is now known to depend on active mechanisms that sense image blur and then take steps to improve the image to include moving retina to reduce the blur and permanently altering ocular dimensions. Among the first changes are an active increase or decrease in choroidal thickness that moves the retina, as shown in laboratory investigations in chickens [63, 64] and primates [65, 66]. Read and associates demonstrated that similar changes in choroidal thickness occur in humans in response to short-term unilateral image blur [62]. The choroid was found to thicken with the myopic defocus condition and to become thinner with the hyperopic defocus [67]. Humans have a diurnal variation in choroidal thickness [51, 68] that is related in magnitude to the baseline thickness of the choroid and systolic blood pressure [51].

9.9 Topography of Choroidal Thickness

In emmetropic eyes the choroid thickness varies topographically within the posterior pole: the choroid was thickest under the fovea with a mean value, and the choroidal thickness decreased rapidly in the nasal direction. The choroidal thickness appears to be thinner in the inferior macula as compared with the superior macula [52, 53, 55, 57]. The inferior peripapillary choroid is thinner than all other quadrants around the nerve [69, 70]. The reason for this finding is not known, but the optic fissure is located in the inferior aspect of the optic cup and is the last part to close during embryology of the eye. Another factor may be this area is in the typical watershed zone in the choroidal circulation. In their study, Ho and associates found that the choroidal thickness increases radially from the optic nerve in all directions in normal emmetropic patients and eventually approaches a plateau [69].

Table 9.1 Predictors of subfoveal choroidal thickness of a group of 145 highly myopic eyes with no macular pathology. Each year of age is associated with a decrease of 1.55 μm of choroidal thickness, while each diopter of myopic refractive error is associated with a decrease of 8.13 μm

| Parameter estimates | | | | | | | |
|---------------------|---------|------------|-------------------------------|---------|-----------------|----|-------|
| Parameter | B | Std. error | 95 % Wald confidence interval | | Hypothesis test | | |
| | | | Lower | Upper | Wald chi-square | df | Sig. |
| (Intercept) | 310.693 | 27.3223 | 257.142 | 364.244 | 129.309 | 1 | <.001 |
| Age | -1.550 | .4064 | -2.347 | -.754 | 14.553 | 1 | <.001 |
| Refraction | 8.133 | 1.8408 | 4.525 | 11.741 | 19.520 | 1 | <.001 |

From Nishida et al. [79]

Dependent variable = subfoveal choroidal thickness

Table 9.2 Predictors of log MAR visual acuity in a group of 145 highly myopic eyes. Only the subfoveal choroidal thickness proved predictive

| Parameter estimates | | | | | | | |
|-------------------------------|--------|------------|-------------------------------|-------|-----------------|----|-------|
| Parameter | B | Std. error | 95 % Wald confidence interval | | Hypothesis test | | |
| | | | Lower | Upper | Wald chi-square | df | Sig. |
| (Intercept) | .287 | .0630 | .163 | .410 | 20.689 | 1 | <.001 |
| Subfoveal choroidal thickness | -.0011 | .0003 | -.002 | .000 | 13.397 | 1 | <.001 |

From Nishida et al. [79]

Dependent variable: logarithm of minimal angle of resolution (logMAR)

9.10 Imaging the Internal Structure of the Choroid

The basement membrane of the choriocapillaris forms the outer layer of Bruch's and the intercapillary pillars of Bruch's membrane separate the vessels of the choriocapillaris. The outer band of reflectivity from the outer retina is ascribed to the RPE, but it is likely that Bruch's membrane and therefore the choriocapillaris are incorporated in the summation of reflection attributed to the RPE obtained with commercially available OCTs. Fong and associates have hypothesized that hyperreflective foci visualized beneath the Bruch's membrane line represent cross sections of feeding and draining arterioles and venules [71]. Larger choroidal vessels have hyporeflective cores with surrounding hyperreflective walls. The luminal diameter of the images probably is proportional but not necessarily exactly equal to the lumen diameter of the corresponding vessel. It is possible that some portion of the outer blood column could be imaged as being part of the wall.

9.11 The Choroid in High Myopia

The thickness of the choroid has been found to vary inversely with the age of the subject and the amount of myopic refractive error (Tables 9.1 and 9.2; Fig. 9.4b). The choroidal thickness varies inversely with the axial length, with the regression models being nearly equivalent to those using refractive error.

This is probably because high myopes seen in a retina clinic are almost always axial myopes; as such this observation might not apply universally to the general pool of high myopes. In the process of becoming highly myopic, the eye appears to expand but does not make additional tissue. For example, the collagen weight of the sclera does not increase with the development of experimental myopia, it actually decreases. The choroid may well be stretched to a certain degree by the development of myopia without the creation of additional vasculature. This determination has not been made yet and would be best modeled over the expanse of the eye and not just the limited area currently imaged with commercial OCT instruments. The decrease in thickness of the choroid in high myopes has, appropriately enough, been called myopic choroidal thinning (Fig. 9.5). The expansion of the eye seems to cause a decrease in the packing density of the photoreceptors [72], with retention of the same visual acuity, because the extension of the axial length also causes a proportional enlargement of the projected image. Although the choroid is thinner, the oxygen requirements per unit area of outer retina may be decreased because of the reduced packing density (Fig. 9.6). However the reduction in thickness of the choroid with age continues in non-myopes and myopes alike. Curiously the diminution in choroidal thickness with age is approximately the same in absolute amounts in high myopes as in eyes that do not have high myopia (Fig. 9.7) [73]. High myopes start out with attenuated thicknesses and progress to remarkably thin or even absent areas of choroid. At some threshold the choroid would have some difficulty in supplying

enough oxygen and other metabolites. From that point the term myopic choroidal atrophy is appropriate [73]. In elderly people without high myopia, the choroid may show reduced thickness in a process known as age-related choroidal atrophy (ARCA) [74]. These patients have normal axial lengths but show tessellation of the fundus, much the same as older high myopes, and beta-zone peripapillary atrophy. Eyes with decreased choroidal thickness as part of ARCA are more

likely to have pseudodrusen, while highly myopic eyes almost never have pseudodrusen. ARCA has been defined as a choroidal thickness of less than 125 μm based on population studies, while myopic choroidal atrophy has not had a thickness definition published.

There is a remarkable dearth of reported histologic information concerning highly myopic eyes. Eyes with early stages of the disease typically are not available for histologic analysis. Animal models of myopia were found to have decreased choriocapillaris density and diameter [18], but there is the lack of the second important variable, aging, in animal studies. Angiographic studies of the choroid with ICG have also found that the choroidal vasculature was altered in highly myopic eyes [75, 76]. A color Doppler ultrasonographic study found that the choroidal circulation was decreased in highly myopic eyes [77]. The choroid of highly myopic patients is significantly thinner than the choroid of normal eyes [73, 78]. As the choroid supplies oxygen and nutrition to the retinal pigment epithelial cells and the outer retina, compromised choroidal circulation may account, in part, for the retinal dysfunction and vision loss that is seen in high myopia.

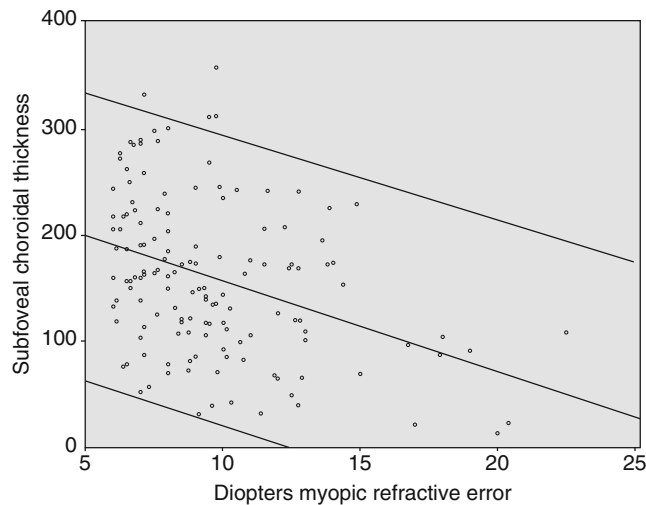


Fig. 9.5 Subfoveal choroidal thickness versus myopic refractive error in a group of 145 highly myopic eyes with no macular pathology. The *trend line* demonstrates the decrease in thickness with increasing refractive error, and the *thinner bordering lines* show the 95 % confidence interval of the trend line. The Y-axis shows the thickness of the choroid in microns

9.12 Biometric Choroidal Changes and Their Clinical Significance

A group of 18 patients (31 eyes), with a mean age of 51.7 years and a mean refractive error of -15.5 D was evaluated with regular SD-OCT. The mean subfoveal choroidal

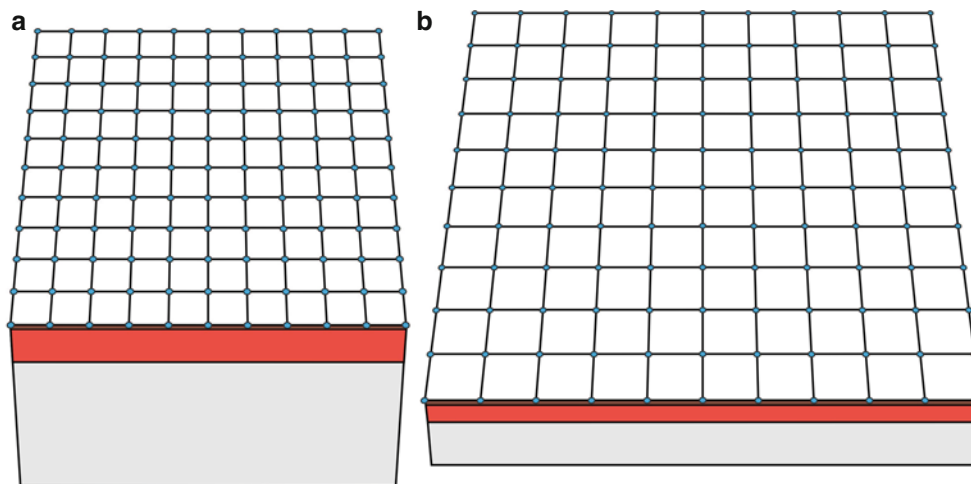


Fig. 9.6 Hypothetical explanation for choroidal thinning and supply of oxygen and metabolites to the retina. (a) In an emmetropic eye the photoreceptors (*blue dots*) have a certain packing density. These are arranged on the retinal pigment epithelium (*brown layer*), which in turn is on the choroid (*orange-red layer*). The sclera is depicted by the gray structure. In a high myope, (b), the posterior pole is stretched, resulting in a lower packing density of the photoreceptors. The choroid

is thinner than an emmetrope. However the ratio of the choroid's ability to supply oxygen and metabolites as compared with the packing density of the photoreceptors may not be adversely affected in high myopes, as evidenced by their good visual function, at least when young. With increasing age the choroid thins, and later in life there is a potential for decreased visual function as a consequence of choroidal atrophy

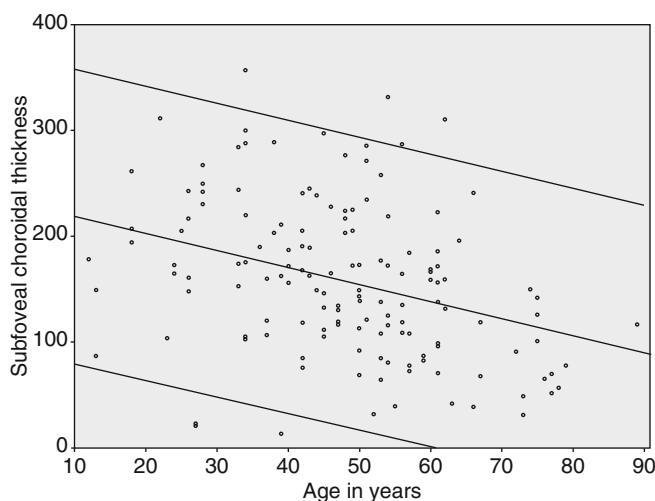


Fig. 9.7 Subfoveal choroidal thickness versus age in a group of 145 highly myopic eyes with no macular pathology. The *trend line* demonstrates the decrease in thickness with age, and the *thinner bordering lines* show the 95 % confidence interval. The Y-axis shows the thickness of the choroid in microns

thickness was only 100.5 μm and was even thinner in older patients and those with greater posterior staphyloma height [91]. The authors defined staphyloma height as the sum of 4 vertical measurements on SD-OCT foveal scans: the distance from the RPE line beneath the fovea to the nasal, temporal, superior, and inferior edges of the OCT image [78]. This method does not mention how the presence, shape, and exact location of the posterior staphyloma were determined. By definition a staphyloma is an outpouching of the eye and is a region where there is an exaggerated curvature of the wall of the eye. Any eye, whether it is myopic or not, is not a flat structure, and as such it should have some “height” as it is defined by this SD-OCT method of measurement. The height measured in this study is a reflection of the posterior curvature of the eye itself and does not necessarily imply any outpouching is present. Conventional SD-OCT allows a relatively good visualization of the choroidal-scleral interface in highly myopic eyes because of the dramatic choroidal thinning [78]. Ikuno and associates reported the scleral interface was undetectable in eyes with a choroidal thickness greater than 300 μm with regular SD-OCT [78]. Visualization would be expected to be dependent on the amount of pigmentation of the RPE and choroid. Another group of 31 patients (55 eyes) with a mean age of 59.7 years and a mean refractive error of -11.9 D was evaluated with EDI-OCT. The mean subfoveal choroidal thickness was 93.2 μm and was negatively correlated with age ($P=0.006$) and refractive error ($P<0.001$) [73]. Eyes with a history of choroidal neovascularization also had a thinner choroid ($P=0.013$), but the patients in this study were treated with photodynamic therapy, which may have damaged the choroid [73]. In this EDI-OCT study, subfoveal choroidal thickness was found to

decrease by 12.7 μm for each decade of life and by 8.7 μm for each diopter of myopia. Nishida and associates evaluated 145 highly myopic eyes and found the choroidal thickness decreased by 15.5 μm per decade of age and 8.13 μm for each diopter of myopia [79].

The visual function in highly myopic patients tends to be more correlated with age than with the amount of myopia [80, 81]. This suggests there are factors other than just the refractive error at play, and given the knowledge that choroidal thickness decreases with both age and myopia, a study was done to look at factors related to visual acuity in highly myopic eyes with no other evident pathology. Two groups of patients, one from New York and the other Japan, were evaluated separately and as a pooled group [79]. Various features were measured in OCT scans by two masked readers. The only predictor of visual acuity, in each of the patient populations and in the pooled data, was the subfoveal choroidal thickness. The thinner the choroid, the less the acuity, although even patients with pronounced thinning of the choroid had what would seem like modest reductions in acuity. Of interest are measures of utility of vision, which show disproportionate loss with even mild changes in acuity. For example, the utility loss of an eye going from 20/20 to 20/40 is about the same as an eye going from 20/40 to 20/200.

In high myopia we are often impressed by the minority of patients with retinal detachment or choroidal neovascularization, because they have sudden loss of acuity. Many patients with high myopia have lesser amounts of acuity loss that individually may not seem all that important. However the number of eyes involved is immense. By analogy in some areas of the world people have deficient intake of iodine. A small minority of people in those areas develop cretinism. A much larger proportion of people have a small decrease in mental function. The cretinism cases are vivid examples; these few people have lost a lot. From a societal standpoint, the many people losing a smaller amount is also important.

9.13 Chorioretinal Atrophy in High Myopia

Regression analysis of choroidal thickness shows a linear trend line descending in proportion to the amount of myopia or age (Figs. 9.5 and 9.7). In general this is a true representation, but there is a lower limit to how thin the choroid theoretically could be and still be functional. Red blood cells have a finite size and the vessels carrying these cells by necessity have to be larger. In OCT images of high myopes, the choroid can be as thin as 15 or so microns (Fig. 9.8). Eyes with choroids this thin have marked alterations of pigmentation to include clumping and rarefaction in adjacent areas. These areas of extreme attenuation of the choroid are seen adjacent to zones of what appears to be complete absence of the choroid. These areas are

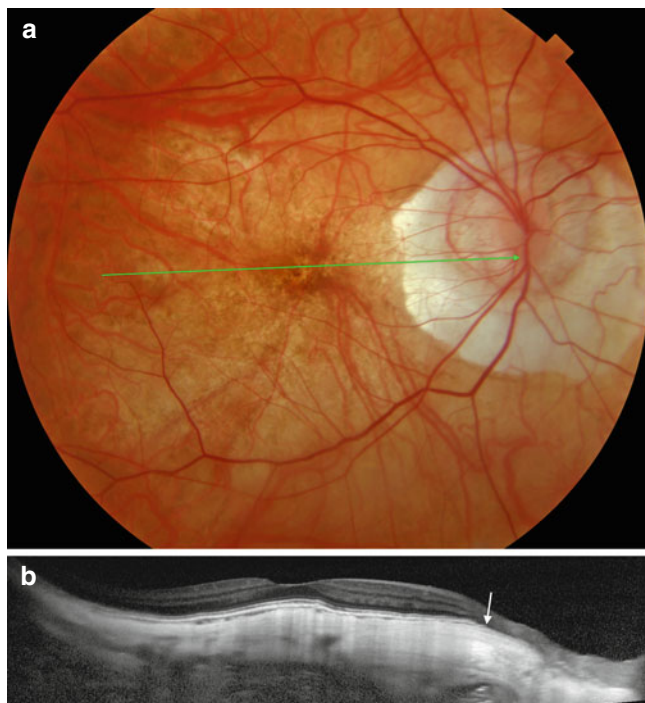


Fig. 9.8 A 70-year-old woman with high myopia. (a) The fundus picture shows attenuation of the choroidal vessels. Note in the central macular region there is a relative paucity of vessels. She is lightly pigmented and therefore doesn't show a prominent tessellated fundus. There is peripapillary atrophy. The *green arrow* shows the location of the section shown in (b). (b) The enhanced depth imaging (EDI) optical coherence tomography (OCT) shows a choroid that is quite thin; the subfoveal choroidal thickness is 14 μm . Note the choroid seems to come to an abrupt end at the border of the normal choroid and the peripapillary atrophy (*arrow*)

brilliantly white because there does not appear to be any extant RPE or choroid, and therefore the underlying sclera is readily visible (Figs. 9.9, 9.10, and 9.11). These areas have attenuation of the overlying retina and have been called chorioretinal atrophy or patchy atrophy. (The term patchy atrophy is misleading in that in the surrounding areas the choroid is also atrophic.) At the border of the chorioretinal atrophy, the choroid does not necessarily gradually thin to nonexistence; it often has a border where a very thin choroid abruptly terminates. This is probably secondary to the anatomic configuration of the remnants of choroid with vessels having either a quantum thickness or not being present at all. With loss of the choroid, there is a concomitant loss of the ability to supply oxygen and metabolites, so the remaining choroidal stroma and the overlying RPE and outer retina appear to wane.

9.14 Intrachoroidal Cavitation

A yellowish-orange lesion typically located immediately inferior to optic nerve occurs in eyes with high myopia [82–89]. This lesion was originally termed peripapillary

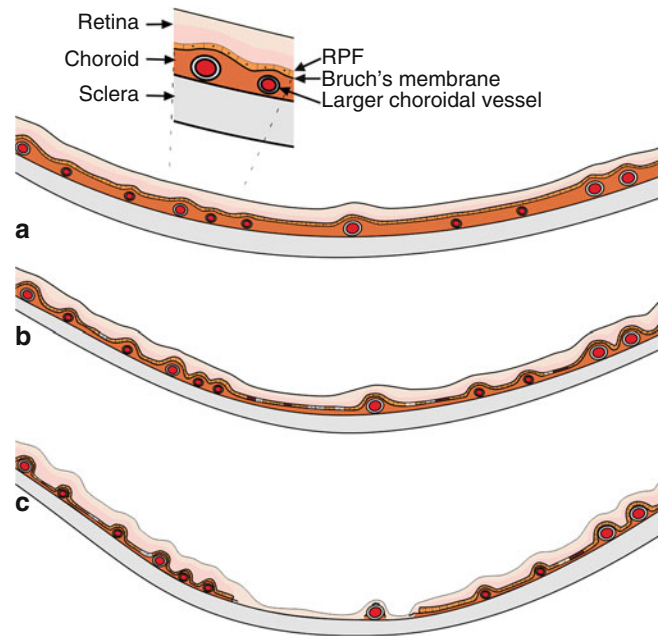


Fig. 9.9 Schematic drawing of choroidal thinning and atrophy. (a) In high myopes the choroid is thinner, with what appears to be attenuation of the middle choroid in particular. The larger choroidal vessels may fill much of the thickness of the choroid. (b) With increasing thinning of the choroid, the larger choroidal blood vessels indent the overlying RPE monolayer. (c) The choroid appears to become so attenuated in older highly myopic patients that it no longer maintains the vitality of the overlying retina and retinal pigment epithelium, or itself for that matter. Areas of absence of the outer retina, RPE, and choroid appear. The remaining tissue is essentially the inner retina. Since this is transparent and the underlying tissue is the sclera, these areas appear *white*

detachment in pathologic myopia because the defect was thought to represent an elevation of the retina and the retinal pigment epithelium (RPE). Peripapillary detachment in pathologic myopia was found in 4.9 % of highly myopic eyes in a series reported by Shimada and coworkers [83]. A steep excavation of the inferior myopic conus was detected adjacent to the peripapillary detachment [84]. Revision of the concepts involving the lesion highlighted some aspects that were inconsistent with the known pathoanatomy of RPE detachments – the lesion appeared to be a cavity but appeared to be located in the choroid [85, 86]. Tateno and colleagues thought the RPE was not separated from the choroid; instead there was a schisis within the choroid [85]. In their case description, Toranzo and colleagues stated, “deep hyporeflectivity was present in the underlying choroid, resembling an intrachoroidal cavitation separating the retinal pigment epithelium from the sclera” [86]. As a consequence they changed the name of the defect to peripapillary intrachoroidal cavitation (ICC) [86]. Wei and associates expanded on the concept of peripapillary ICC and proposed a complex of forces composed of “posterior expansion force, the vitreous traction force, and the vitreous fluid dynamics determine the size and shape of the lesion” [87]. Investigation of a series of 16 eyes

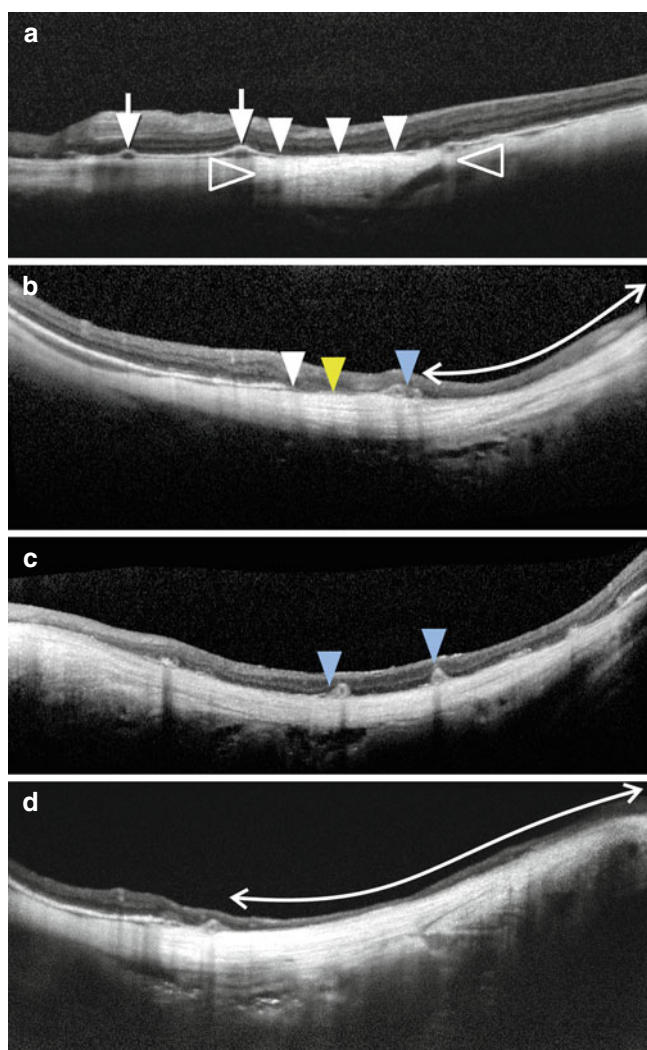


Fig. 9.10 OCT examples of advanced choroidal atrophy in high myopia. (a) The choroid is attenuated in this eye and two larger choroidal vessels (*arrows*) are seen elevating the RPE. Some authors have called these elevations “choroidal microfolds,” which is clearly incorrect since the choroid is not folded. In areas of loss of the RPE, there is increased light transmission to deeper layers (*open arrowheads*). Within this zone what appears to be Bruch’s membrane is seen (*arrowheads*). (b) With more profound loss of the choroid, the RPE terminates leaving a vestige of Bruch’s membrane (*white arrowhead*) and remnants of Bruch’s membrane (*yellow arrowhead*). Around a larger choroidal vessel, there appears to be residual portions of associated choroidal stroma (*blue arrowhead*). The *double-ended white arrow* shows a stretch of the posterior pole without any visible vascularized choroid. Note the loss of substance and laminations in the overlying retina. (c) This eye shows a nearly complete loss of the choroid in the region of the OCT scan. There are two remaining larger choroidal vessels with small vestiges of choroidal tissue (*blue arrowheads*). (d) In an eye with more chronic loss of the choroid, as shown by the extent of the *double-ended white arrow*, the overlying retina is remarkably thinned

with peripapillary ICC using EDI-OCT and SS-OCT showed an interesting anatomic configuration [90]. The sclera in the region of the conus was displaced posteriorly and the backwards deflection of the sclera continued into the region of the

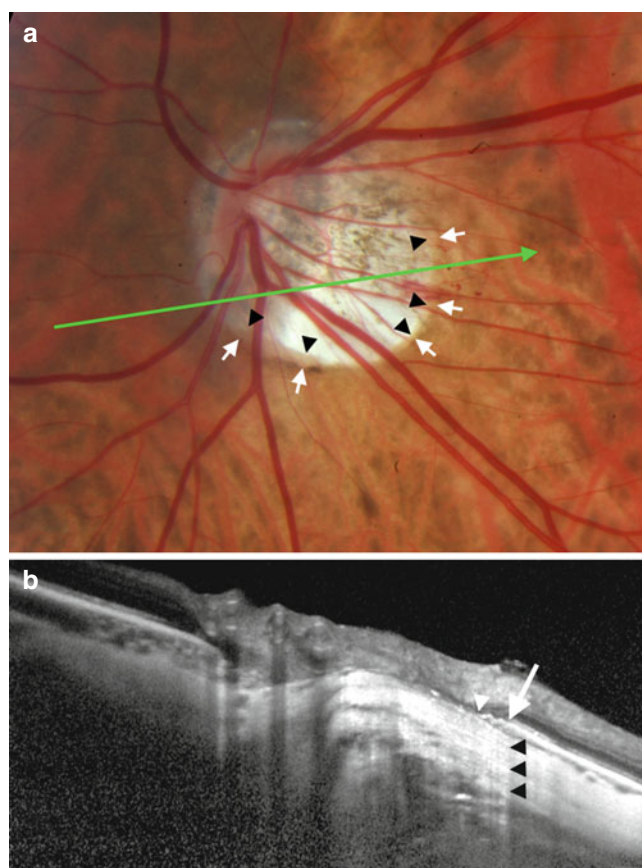


Fig. 9.11 Tilted disc and conus in a high myope. The infrared scanning laser image was projected onto the color picture to be able to accurately locate the scan line shown as the *green arrow*. (a) This eye shows a tilted disc and profound atrophy within a conus inferotemporal to the disc. At the outer border of the conus are two concentric curves. The outer one (*white arrows*) is where the orange color terminates, and the second is the continuation of a more subtle zone of shading prior to the intensely reflective inner zone of the conus. This boundary is shown by the *black arrowheads*. (b) The termination of the orange color corresponds to the *white arrow*. Note the increased penetration of light posterior to this zone, as demarcated by the *black arrowheads*. These signs are taken to mean the RPE stops, or at least becomes attenuated, at this juncture. There is a thinner curved structure that stops nasally (*white arrowhead*), and this structure appears to be the termination of Bruch’s membrane. The termination of this layer corresponds to the line demarcated by the *black arrowheads* in the color photograph

ICC. The overall curvature of the retina, RPE, and Bruch’s membrane complex was seen to be relatively unaffected over the region of the ICC. The cavitation was created by the expansion of the distance between the inner wall of the sclera and the posterior surface of Bruch’s membrane. There also appeared to be alterations of the anatomy around the optic nerve caused by the posterior displacement of the sclera (Fig. 9.12). A full thickness defect in the retina was found in one quarter of the eyes at the border of the conus.

The eye ordinarily is inflated by its intraocular pressure with the wall of the eye acting as the outer barrier, resisting outward expansion. The ability of the wall of the eye to resist

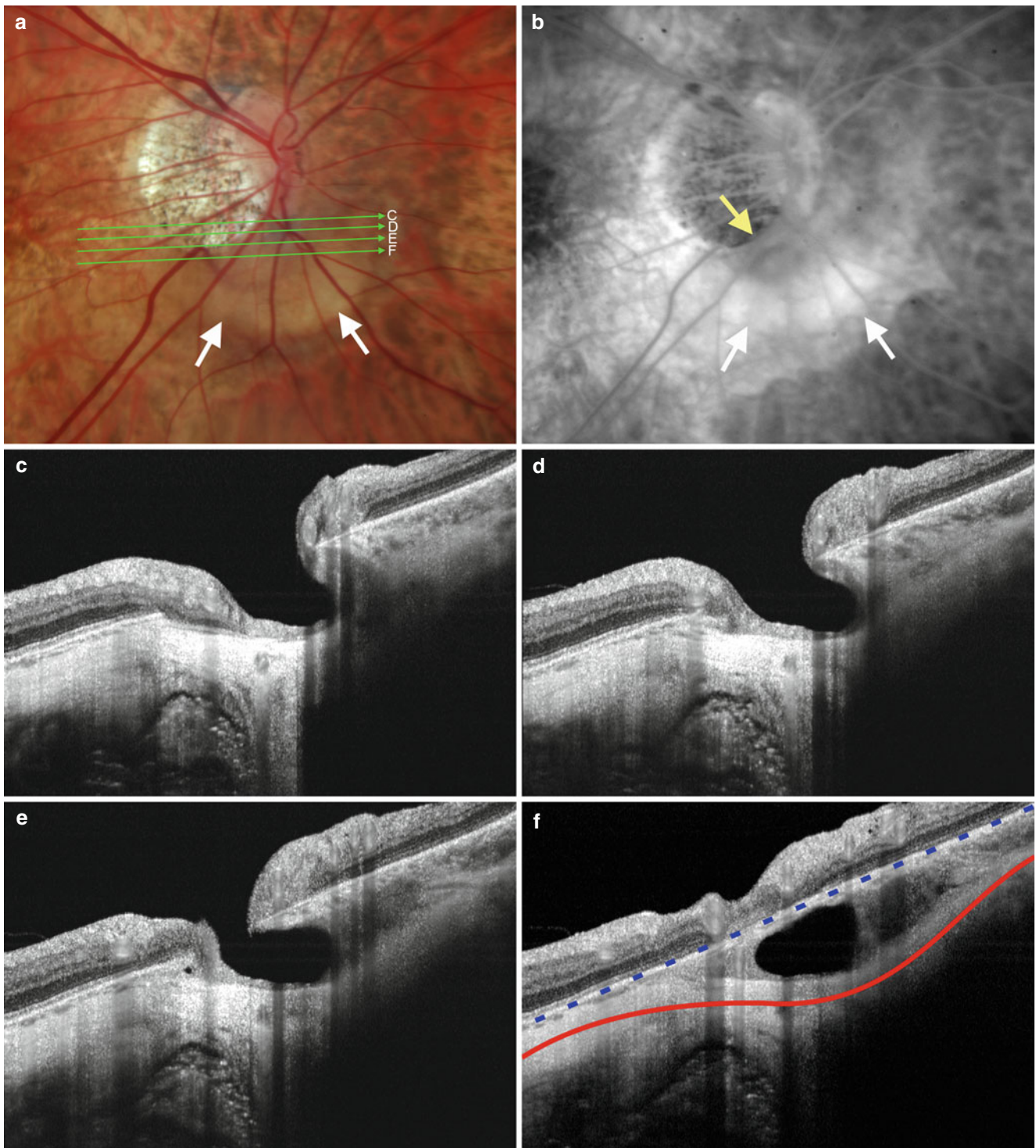


Fig. 9.12 (a) This color photograph shows the yellow-orange region of the intrachoroidal cavitation (*white arrows*). The *green arrows* show the locations of subsequent optical coherence tomography (OCT) sections. (b) A fluorescein angiogram shows a modest late collection of dye within the cavity. Note the edge of the retinal defect is more clearly evident than in the color photograph. (c–f) Successive serial sections using swept-source OCT showing the

inner retinal defect and the extension of the cavitation into the choroid. There is a veil of tissue extending through the thickness of the choroid at the border of the cavitation. In (f) note that the hyperreflective band corresponding to the retinal pigment epithelium is nearly straight, as illustrated by the *blue dashed line* overlay. The sclera shows an outbowing posteriorly with the *red line* at the center point thickness

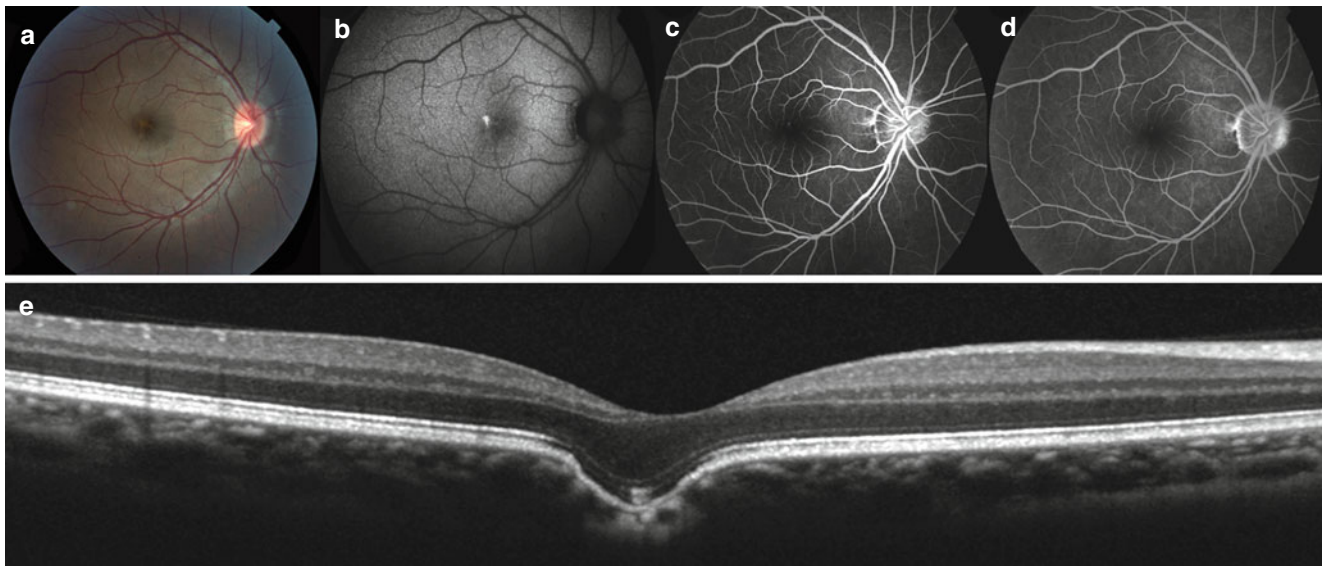


Fig. 9.13 A 33-year-old man with a conforming focal choroidal excavation. (a) Color photograph of the right eye reveals a perifoveal yellowish spot consistent with a small vitelliform lesion. (b) Fundus autofluorescent image of the right eye reveals a focal area of hyperautofluorescence corresponding to the vitelliform material. Late venous phase (c) and recirculation phase (d) fluorescein angiographic images

reveal a focal hyperfluorescent spot supratemporal to the fovea. (e) Spectral-domain optical coherence tomographic scan through the fovea reveals a conforming focal choroidal excavation with a small area of outer retinal hyperreflectivity corresponding to the vitelliform lesion (a) (From Vance et al. [98])

deformation is related to its inherent elasticity and its thickness. Over normal expanses, the wall of the eye is composed of the retina, RPE, Bruch's membrane, the choroid, and sclera. In the region of the conus there is no choroid, RPE, or outer retina. The inner retina can be very attenuated. The underlying sclera is thinned in eyes with high myopia, particularly in the region of the conus. The comparatively thin eyewall in the area of the conus is exposed to the same force per unit area from intraocular pressure as other areas in the eye and therefore is more likely to experience deformation as compared with regions of the eye having all layers intact. Since the sclera has some stiffness, the posterior deformation continues into surrounding normal areas, thus causing the separation or cavitation in the choroid. There appears to be more staphylomatous expansion of these eyes at the inferotemporal portion of the disc, possibly explaining the frequent inferior location of peripapillary ICC [90].

This same mechanical defect potentially can exist in other regions and may offer explanation for similar cavitations in the macular region of high myopes. These cavitations occurred in the posterior pole of eyes with neighboring areas of loss of the choroid and overlying RPE [91]. The posterior displacement of the sclera continued into relatively normal surrounding areas appears to be the cause of macular ICC. Almost $\frac{1}{4}$ of eyes with ICC have a retinal defect located near the border between the attenuated retina and the surrounding normal retina. In some patient fluid dissecting under the retina has resulted in a localized retinal detachment.

9.15 Focal Choroidal Excavation

Eyes with myopia generally have decreasing choroidal thickness in proportion with their amount of myopic refractive error. An unusual group of patients have what is termed focal choroidal cavitation and entity in which there is a localized loss of choroidal thickness within the macula [92–94]. These patients are generally myopic with some being highly myopic. Affected eyes have solitary localized areas that usually show pigmentary alterations, but the cavitation itself may be difficult to see by biomicroscopy. The cavitations are readily visible using OCT (Fig. 9.13). These areas show hypofluorescence during both fluorescein and indocyanine green angiography and localized hypoautofluorescence. In a group of 10 eyes, EDI-OCT was performed in 6, and these showed a choroid that appeared to be abnormally thick in the regions surrounding the excavation [94]. The choroid was thin at the excavation and the choroidal-scleral junction showed no abnormalities. The excavation was thought to represent a localized hypoplastic region.

9.16 Future Trends for Research

There is much to be learned about the choroid in myopia. The process of emmetropization appears to be misdirected or abnormal in high myopes, and is mediated in part by the choroid.

Yet in high myopia the choroid becomes increasingly abnormal. The influence these changes have on the progression of myopia is not known. The ability to image the thickness of the choroid using OCT is relatively recent, so there is an absence of any long-term data. Classification systems for the posterior pole changes in high myopia have relied on ophthalmoscopy alone. Integrating choroidal thickness into the classification system would introduce a variable that has biologic plausibility to both influence visual function and preserve associated tissue. Decreased choroidal perfusion also may be related to secondary abnormalities seen in high myopia such as choroidal neovascularization as discussed in a separate chapter in this text.

There are many research efforts aiming to reduce the progression of myopia, but reduction of the choroidal effects related to myopia would obviate many of the common reasons for visual loss in the first place. Thickening of the choroid is seen in inflammatory diseases [95] and in central serous chorioretinopathy [96]. It is possible that pharmacologic manipulation can influence choroidal thickness. Oral sildenafil caused an increase in choroidal thickness in normal volunteers [97, 98]. Corticosteroids are associated with central serous chorioretinopathy and may have an associated effect of increasing choroidal thickness. One older high myope was imaged and found to have a thickened choroid. Interestingly, she had a kidney transplant in the past and had been treated with oral prednisone for many years (Fig. 9.14).

9.16.1 Potential Use of Choroidal Thickness in Grading Myopic Fundus Changes

Epidemiologic studies use grading systems to classify and quantitate incidence and severity of myopic changes in populations. There are key attributes required of any grading system to be useful. The grading system should be exhaustive of all possibilities of disease expression, the stages in the grading system should be relevant to important stages of the disease process and be based on objective information, and the results should be accurate and reproducible. Current classification systems grade myopia based on attributes such as tessellation, diffuse atrophy, patchy atrophy, lacquer cracks, and Fuchs spots. This list does not represent an exhaustive tabulation of possibilities, the grading of any of these attributes is quite subjective, and the presence of these findings is dependent on the population being graded. For example, tessellation is the presence of a striped pattern caused by visualization of larger choroidal blood vessels contrasted by intervening pigment in the outer choroid. Eyes with the tessellated fundus appearance have thinner choroids than eyes with a normal fundus appearance. Thinning of the choroid is associated with loss of the middle layer, allowing visualization of deeper layers. The contrast between the vessels and

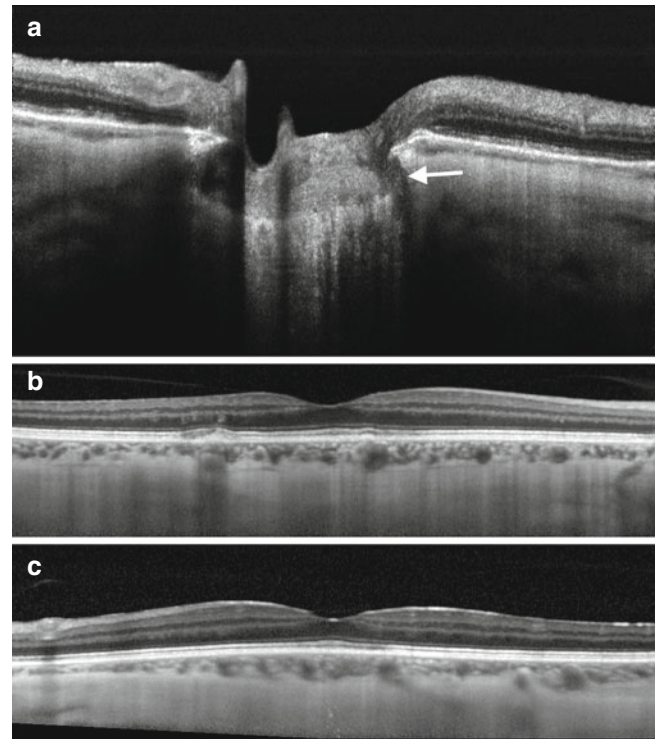


Fig. 9.14 (a) This highly myopic, 66-year-old woman had typical features of a high myope, including a dehiscence in the lamina cribrosa as seen in this swept-source OCT scan (*arrow*), but her choroid was unexpectedly thick. (b, c) Given her age and axial length, she would be expected to have a subfoveal choroidal thickness of about 50 μm . Instead her choroid was nearly 200 μm thick. She had a kidney transplantation and was using oral prednisone for many years to prevent rejection. Corticosteroids are a risk factor for central serous chorioretinopathy, a condition that causes choroidal thickening. However the number of vessels within this patient's choroid appears to be grossly normal, which is different from a typical older high myope in which the choroid usually has a reduced number of vessels (e.g., see Fig. 9.10). One case does not prove anything, but these findings raise interesting possibilities

the pigmented portions depends in part on how much pigment is present. A highly pigmented person would have dark regions bordered by vessels while a person who is of Northern European extraction would not. For any given amount of choroidal change, a highly pigmented person would be more likely to appear to be tessellated. Fuchs spots are pigmented scars left by choroidal neovascularization. It is common for patients with blonde fundi to not develop a deeply pigmented scar after choroidal neovascularization and for eyes treated with anti-VEGF agents to not develop significant scars in the first place. In the case of either tessellation or Fuchs spots, the grading of presence or absence is dependent on factors other than disease severity. Currently the only means we have to clinically evaluate the choroidal thickness in high myopes is optical coherence tomography. It would be helpful to have histologic correlation to what is visualized.

Acknowledgement Sarah Mjeren, MD, provided assistance in assembling the references.

References

- Parver LM, Auker C, Carpenter DO. Choroidal blood flow as a heat dissipating mechanism in the macula. *Am J Ophthalmol*. 1980; 89(5):641–6.
- Wangsa-Wirawan ND, Linsenmeier RA. Retinal oxygen: fundamental and clinical aspects. *Arch Ophthalmol*. 2003;121(4): 547–57.
- Parver LM, Auker C, Carpenter DO. Choroidal blood flow as a heat dissipating mechanism in the macula. *Am J Ophthalmol*. 1980;84: 641–6.
- Yuan X, Gu X, Crabb JS, et al. Quantitative proteomics: comparison of the macular Bruch membrane/choroid complex from age-related macular degeneration and normal eyes. *Mol Cell Proteomics*. 2010;9:1031–46.
- Nickla DL, Wallman J. The multifunctional choroid. *Prog Retin Eye Res*. 2010;29(2):144–68.
- Sellheyer K. Development of the choroid and related structures. *Eye (Lond)*. 1990;4(Pt 2):255–61.
- Mund ML, Rodrigues MM, Fine BS. Light and electron microscopic observations on the pigmented layers of the developing human eye. *Am J Ophthalmol*. 1972;73(2):167–82.
- Meriney SD, Pilar G. Cholinergic innervation of the smooth muscle cells in the choroid coat of the chick eye and its development. *J Neurosci*. 1987;7(12):3827–39.
- Schroedl F, Brehmer A, Neuhuber WL, et al. The normal human choroid is endowed with a significant number of lymphatic vessel endothelial hyaluronate receptor 1 (LYVE-1)-positive macrophages. *Invest Ophthalmol Vis Sci*. 2008;49(12):5222–9.
- May CA. Non-vascular smooth muscle cells in the human choroid: distribution, development and further characterization. *J Anat*. 2005;207(4):381–90.
- Poukens V, Glasgow BJ, Demer JL. Nonvascular contractile cells in sclera and choroid of humans and monkeys. *Invest Ophthalmol Vis Sci*. 1998;39(10):1765–74.
- Flugel-Koch C, May CA, Lutjen-Drecoll E. Presence of a contractile cell network in the human choroid. *Ophthalmologica*. 1996; 210(5):296–302.
- de Hoz R, Ramirez AI, Salazar JJ, et al. Substance P and calcitonin gene-related peptide intrinsic choroidal neurons in human choroidal whole-mounts. *Histol Histopathol*. 2008;23(10):1249–58.
- Saint-Geniez M, Kurihara T, Sekiyama E, et al. An essential role for RPE-derived soluble VEGF in the maintenance of the choriocapillaris. *Proc Natl Acad Sci U S A*. 2009;106(44):18751–6.
- Bernstein MH, Hollenberg MJ. Fine structure of the choriocapillaris and retinal capillaries. *Invest Ophthalmol*. 1965;4(6):1016–25.
- Federman JL. The fenestrations of the choriocapillaris in the presence of choroidal melanoma. *Trans Am Ophthalmol Soc*. 1982;80: 498–516.
- Peters S, Heiduschka P, Julien S, et al. Ultrastructural findings in the primate eye after intravitreal injection of bevacizumab. *Am J Ophthalmol*. 2007;143(6):995–1002.
- Hirata A, Negi A. Morphological changes of choriocapillaris in experimentally induced chick myopia. *Graefes Arch Clin Exp Ophthalmol*. 1998;236:132–7.
- Rutnin U, Schepens CL. Fundus appearance in normal eyes. II. The standard peripheral fundus and developmental variations. *Am J Ophthalmol*. 1967;64(5):840–52.
- Haab O. Atlas and Grundriss der Ophthalmoscopie und ophthalmoscopischen Diagnostik. 3rd ed. Munchen Verlag von J. F. Lehmann. 1900, Figure 80, p. 90, hintere Vortexvenen.
- Guyer DR, Schachat AP, Green WR. The choroid: structural considerations. In: Ryan SJ, editor. *Retina*. 4th ed. Philadelphia: Mosby; 2006. p. 34–41.
- Hayreh SS. In vivo choroidal circulation and its watershed zones. *Eye (Lond)*. 1990;4(Pt 2):273–89.
- Maepea O. Pressures in the anterior ciliary arteries, choroidal veins and choriocapillaris. *Exp Eye Res*. 1992;54(5):731–6.
- Flower RW, Fryczkowski AW, McLeod DS. Variability in choriocapillaris blood flow distribution. *Invest Ophthalmol Vis Sci*. 1995;36:1247–58.
- Chen JC, Fitzke FW, Pauleikhoff D, Bird AC. Functional loss in age-related Bruch's membrane change with choroidal perfusion defect. *Invest Ophthalmol Vis Sci*. 1992;33:334–40.
- Hayreh SS. The blood supply of the optic nerve head and the evaluation of it – myth and reality. *Prog Retin Eye Res*. 2001;20(5): 563–93.
- Alm A, Bill A. Ocular and optic nerve blood flow at normal and increased intraocular pressures in monkeys (*Macaca irus*): a study with radioactively labelled microspheres including flow determinations in brain and some other tissues. *Exp Eye Res*. 1973;15(1):15–29.
- Friedman E. Choroidal blood flow. Pressure-flow relationships. *Arch Ophthalmol*. 1970;83(1):95–9.
- Kiel JW, van Heuven WA. Ocular perfusion pressure and choroidal blood flow in the rabbit. *Invest Ophthalmol Vis Sci*. 1995;36(3): 579–85.
- Polak K, Luksch A, Berisha F, et al. Altered nitric oxide system in patients with open-angle glaucoma. *Arch Ophthalmol*. 2007;125(4): 494–8.
- Lutjen-Drecoll E. Choroidal innervation in primate eyes. *Exp Eye Res*. 2006;82(3):357–61.
- Polska E, Simader C, Weigert G, et al. Regulation of choroidal blood flow during combined changes in intraocular pressure and arterial blood pressure. *Invest Ophthalmol Vis Sci*. 2007;48(8): 3768–74.
- Riva CE, Titze P, Hero M, et al. Choroidal blood flow during isometric exercises. *Invest Ophthalmol Vis Sci*. 1997;38(11):2338–43.
- Riva CE, Titze P, Hero M, Petrig BL. Effect of acute decreases of perfusion pressure on choroidal blood flow in humans. *Invest Ophthalmol Vis Sci*. 1997;38(9):1752–60.
- Houssier M, Raoul W, Lavalette S, et al. CD36 deficiency leads to choroidal involution via COX2 down-regulation in rodents. *PLoS Med*. 2008;5(2):e39.
- Fujiwara T, Imamura Y, Giovinazzo VJ, Spaide RF. Fundus autofluorescence and optical coherence tomographic findings in acute zonal occult outer retinopathy. *Retina*. 2010;30(8):1206–16.
- Geiser MH, Bonvin M, Quibel O. Corneal and retinal temperatures under various ambient conditions: a model and experimental approach. *Klin Monbl Augenheilkd*. 2004;221(5):311–4.
- Biesemeier A, Schraermeyer U, Eibl O. Chemical composition of melanosomes, lipofuscin and melanolipofuscin granules of human RPE tissues. *Exp Eye Res*. 2011;93:29–39.
- Ulshafer RJ, Allen CB, Rubin ML. Distributions of elements in the human retinal pigment epithelium. *Arch Ophthalmol*. 1990;108: 113–7.
- Biesemeier A, Julien S, Kokkinou D, Schraermeyer U, Eibl O. A low zinc diet leads to loss of Zn in melanosomes of the RPE but not in melanosomes of the choroidal melanocytes. *Metallomics*. 2012;4:323–32.
- Geeraets WJ, Berry ER. Ocular spectral characteristics as related too hazards from lasers and other light sources. *Am J Ophthalmol*. 1968;66:15–20.
- Ketterer SG, Wiegand BD. Hepatic clearance of indocyanine green. *Clin Res*. 1959;7:289.
- Hayashi K, Hasegawa T, Tokoro T, Delaey JJ. Value of indocyanine green angiography in the diagnosis of occult choroidal neovascular membrane. *Jpn J Ophthalmol*. 1988;42:827–9.

44. Hewick SA, Fairhead AC, Culy JC, Atta HR. A comparison of 10 MHz and 20 MHz ultrasound probes in imaging the eye and orbit. *Br J Ophthalmol*. 2004;88(4):551–5.
45. Hoffer KJ. Ultrasound velocities for axial eye length measurement. *J Cataract Refract Surg*. 1994;20(5):554–62.
46. Spaide RF, Koizumi H, Pozzoni MC. Enhanced depth imaging spectral-domain optical coherence tomography. *Am J Ophthalmol*. 2008;146(4):496–500.
47. Chinn SR, Swanson EA, Fujimoto JG. Optical coherence tomography using a frequency-tunable optical source. *Opt Lett*. 1997;22(5):340–2.
48. Choma M, Sarunic M, Yang C, Izatt J. Sensitivity advantage of swept source and Fourier domain optical coherence tomography. *Opt Express*. 2003;11(18):2183–9.
49. Branchini L, Regatieri CV, Flores-Moreno I, et al. Reproducibility of choroidal thickness measurements across three spectral domain optical coherence tomography systems. *Ophthalmology*. 2012;119:119–23.
50. Ikuno Y, Maruko I, Yasuno Y, et al. Reproducibility of retinal and choroidal thickness measurements in enhanced depth imaging and high-penetration optical coherence tomography. *Invest Ophthalmol Vis Sci*. 2011;52(8):5536–40.
51. Tan CS, Ouyang Y, Ruiz H, Sadda SR. Diurnal variation of choroidal thickness in normal, healthy subjects. *Invest Ophthalmol Vis Sci*. 2012;53(1):261–6.
52. Manjunath V, Taha M, Fujimoto JG, Duker JS. Choroidal thickness in normal eyes measured using Cirrus HD optical coherence tomography. *Am J Ophthalmol*. 2010;150(3):325–9.e1.
53. Hirata M, Tsujikawa A, Matsumoto A, et al. Macular choroidal thickness and volume in normal subjects measured by swept-source optical coherence tomography. *Invest Ophthalmol Vis Sci*. 2011;52(8):4971–8.
54. Margolis R, Spaide RF. A pilot study of enhanced depth imaging optical coherence tomography of the choroid in normal eyes. *Am J Ophthalmol*. 2009;147(5):811–5.
55. Ikuno Y, Kawaguchi K, Nouchi T, Yasuno Y. Choroidal thickness in healthy Japanese subjects. *Invest Ophthalmol Vis Sci*. 2010;51(4):2173–6.
56. Benavente-Perez A, Hosking SL, Logan NS, Bansal D. Reproducibility-repeatability of choroidal thickness calculation using optical coherence tomography. *Optom Vis Sci*. 2010;87(11):867–72.
57. Esmaeelpour M, Povazay B, Hermann B, et al. Three-dimensional 1060-nm OCT: choroidal thickness maps in normal subjects and improved posterior segment visualization in cataract patients. *Invest Ophthalmol Vis Sci*. 2010;51(10):5260–6.
58. Li XQ, Larsen M, Munch IC. Subfoveal choroidal thickness in relation to sex and axial length in 93 Danish university students. *Invest Ophthalmol Vis Sci*. 2011;52(11):8438–41.
59. Feeney-Burns L, Burns RP, Gao CL. Age-related macular changes in humans over 90 years old. *Am J Ophthalmol*. 1990;109(3):265–78.
60. Sarks SH. Ageing and degeneration in the macular region: a clinicopathological study. *Br J Ophthalmol*. 1976;60(5):324–41.
61. Ramrattan RS, van der Schaft TL, Mooy CM, et al. Morphometric analysis of Bruch's membrane, the choriocapillaris, and the choroid in aging. *Invest Ophthalmol Vis Sci*. 1994;35(6):2857–64.
62. Read SA, Collins MJ, Sander BP. Human optical axial length and defocus. *Invest Ophthalmol Vis Sci*. 2010;51(12):6262–9.
63. Wallman J, Wildsoet C, Xu A, et al. Moving the retina: choroidal modulation of refractive state. *Vision Res*. 1995;35(1):37–50.
64. Wildsoet C, Wallman J. Choroidal and scleral mechanisms of compensation for spectacle lenses in chicks. *Vision Res*. 1995;35(9):1175–94.
65. Troilo D, Nickla DL, Wildsoet CF. Choroidal thickness changes during altered eye growth and refractive state in a primate. *Invest Ophthalmol Vis Sci*. 2000;41(6):1249–58.
66. Hung LF, Wallman J, Smith 3rd EL. Vision-dependent changes in the choroidal thickness of macaque monkeys. *Invest Ophthalmol Vis Sci*. 2000;41(6):1259–69.
67. Rohrer K, Frueh BE, Walti R, et al. Comparison and evaluation of ocular biometry using a new noncontact optical low-coherence reflectometer. *Ophthalmology*. 2009;116(11):2087–92.
68. Brown JS, Flitcroft DI, Ying GS, et al. In vivo human choroidal thickness measurements: evidence for diurnal fluctuations. *Invest Ophthalmol Vis Sci*. 2009;50(1):5–12.
69. Ho J, Branchini L, Regatieri C, et al. Analysis of normal peripapillary choroidal thickness via spectral domain optical coherence tomography. *Ophthalmology*. 2011;118(10):2001–7.
70. Tanabe H, Ito Y, Terasaki H. Choroid is thinner in inferior region of optic disks of normal eyes. *Retina*. 2012;32(1):134–9.
71. Fong AH, Li KK, Wong D. Choroidal evaluation using enhanced depth imaging spectral-domain optical coherence tomography in Vogt-Koyanagi-Harada disease. *Retina*. 2011;31(3):502–9.
72. Chui TY, Song H, Burns SA. Individual variations in human cone photoreceptor packing density: variations with refractive error. *Invest Ophthalmol Vis Sci*. 2008;49(10):4679–87.
73. Fujiwara T, Imamura Y, Margolis R, et al. Enhanced depth imaging optical coherence tomography of the choroid in highly myopic eyes. *Am J Ophthalmol*. 2009;148(3):445–50.
74. Spaide RF. Age-related choroidal atrophy. *Am J Ophthalmol*. 2009;147:801–10.
75. Moriyama M, Ohno-Matsui K, Futagami S, et al. Morphology and long-term changes of choroidal vascular structure in highly myopic eyes with and without posterior staphyloma. *Ophthalmology*. 2007;114(9):1755–62.
76. Quaranta M, Arnold J, Coscas G, et al. Indocyanine green angiographic features of pathologic myopia. *Am J Ophthalmol*. 1996;122(5):663–71.
77. Akyol N, Kukner AS, Ozdemir T, Esmerligil S. Choroidal and retinal blood flow changes in degenerative myopia. *Can J Ophthalmol*. 1996;31(3):113–9.
78. Ikuno Y, Tano Y. Retinal and choroidal biometry in highly myopic eyes with spectral-domain optical coherence tomography. *Invest Ophthalmol Vis Sci*. 2009;50(8):3876–80.
79. Nishida Y, Fujiwara T, Imamura Y, et al. Choroidal thickness and visual acuity in highly myopic eyes. *Retina*. 2012;32(7):1229–36.
80. Saw SM, Gazzard G, Shih-Yen EC, Chua WH. Myopia and associated pathological complications. *Ophthalmic Physiol Opt*. 2005;25(5):381–91.
81. Vongphanit J, Mitchell P, Wang JJ. Population prevalence of tilted optic disks and the relationship of this sign to refractive error. *Am J Ophthalmol*. 2002;133(5):679–85.
82. Freund KB, Ciardella AP, Yannuzzi LA, et al. Peripapillary detachment in pathologic myopia. *Arch Ophthalmol*. 2003;121:197–204.
83. Shimada N, Ohno-Matsui K, Nishimuta A, Tokoro T, Mochizuki M. Peripapillary changes detected by optical coherence tomography in eyes with high myopia. *Ophthalmology*. 2007;114:2070–6.
84. Shimada N, Ohno-Matsui K, Yoshida T, et al. Characteristics of peripapillary detachment in pathologic myopia. *Arch Ophthalmol*. 2006;124:46–52.
85. Tateno H, Takahashi K, Fukuchi T, Yamazaki Y, Sho K, Matsumura M. Choroidal schisis around the optic nerve in myopic eyes evaluated by optical coherence tomography. *Jpn J Clin Ophthalmol*. 2005;59:327–31.
86. Toranzo J, Cohen SY, Erginay A, Gaudric A. Peripapillary intrachoroidal cavitation in myopia. *Am J Ophthalmol*. 2005;140:731–2.
87. Wei YH, Yang CM, Chen MS, Shih YF, Ho TC. Peripapillary intrachoroidal cavitation in high myopia: reappraisal. *Eye (Lond)*. 2009;23:141–4.
88. Forte R, Pascotto F, Cennamo G, de Crecchio G. Evaluation of peripapillary detachment in pathologic myopia with en face optical coherence tomography. *Eye (Lond)*. 2008;22:158–61.

89. Shimada N, Ohno-Matsui K, Iwanaga Y, Tokoro T, Mochizuki M. Macular retinal detachment associated with peripapillary detachment in pathologic myopia. *Int Ophthalmol*. 2009;29:99–102.
90. Spaide RF, Akiba M, Ohno-Matsui K. Evaluation of peripapillary intrachoroidal cavitation with swept source and enhanced depth imaging optical coherence tomography. *Retina*. 2012;32:1037–44.
91. Ohno-Matsui K, Akiba M, Moriyama M, Ishibashi T, Hirakata A, Tokoro T. Intrachoroidal cavitation in macular area of eyes with pathologic myopia. *Am J Ophthalmol*. 2012;154(2):382–93.
92. Jampol LM, Shankle J, Schroeder R, Tornambe P, Spaide RF, Hee MR. Diagnostic and therapeutic challenges. *Retina*. 2006;26(9):1072–6.
93. Wakabayashi Y, Nishimura A, Higashide T, Ijiri S, Sugiyama K. Unilateral choroidal excavation in the macula detected by spectral-domain optical coherence tomography. *Acta Ophthalmol*. 2010;88(3):e87–91.
94. Margolis R, Mukkamala SK, Jampol LM, Spaide RF, Ober MD, Sorenson JA, Gentile RC, Miller JA, Sherman J, Freund KB. The expanded spectrum of focal choroidal excavation. *Arch Ophthalmol*. 2011;129(10):1320–5.
95. Maruko I, Iida T, Sugano Y, Oyamada H, Sekiryu T, Fujiwara T, Spaide RF. Subfoveal choroidal thickness after treatment of Vogt-Koyanagi-Harada disease. *Retina*. 2011;31:510–7.
96. Imamura Y, Fujiwara T, Margolis R, Spaide RF. Enhanced depth imaging optical coherence tomography of the choroid in central serous chorioretinopathy. *Retina*. 2009;29:1469–73.
97. Harris A, Kagemann L, Ehrlich R, Ehrlich Y, López CR, Purvin VA. The effect of sildenafil on ocular blood flow. *Br J Ophthalmol*. 2008;92:469–73.
98. Vance SK, Imamura Y, Freund KB. The effects of sildenafil citrate on choroidal thickness as determined by enhanced depth imaging optical coherence tomography. *Retina*. 2011;31:332–5.
99. Ohno-Matsui K, Akiba M, Moriyama M, Ishibashi T, Tokoro T, Spaide RF. Imaging retrobulbar subarachnoid space around optic nerve by swept-source optical coherence tomography in eyes with pathologic myopia. *Invest Ophthalmol Vis Sci*. 2011;52:9644–50.